*Inorg. Chem.* **2007**, *46*, 3072–3082


# DNA Binding Studies of Novel Copper(II) Complexes Containing L-Tryptophan as Chiral Auxiliary: In Vitro Antitumor Activity of Cu–$Sn_2$ Complex in Human Neuroblastoma Cells

**Mala Chauhan,[†] Kakoli Banerjee,[‡] and Farukh Arjmand*[,†]**

*Department of Chemistry, Aligarh Muslim University, Aligarh-202002, India, and National Institute of Immunology, New Delhi, India*

Received September 15, 2006

Novel trinuclear complexes $C_{23}H_{31}N_6O_6CuSn_2Cl_5$ [**1**], $C_{23}H_{31}N_6O_6CuZr_2Cl_5$ [**2**], $C_{23}H_{31}N_6O_6ZnSn_2Cl_5$ [**3**], and $C_{23}H_{31}N_6O_6ZnZr_2Cl_5$ [**4**] were synthesized and characterized by spectroscopic (IR, $^1H$, $^{13}C$, 2D COSY, and $^{119}Sn$ NMR, EPR, UV–vis, ESI-MS) and analytical methods. In complexes **1**–**4**, the geometry of copper and zinc metal ions were described as square-based pyramidal with L-tryptophan coordinated to copper/zinc via carboxylate group while Sn/Zr was present in the hexacoordinate environment. The interaction of **1** and **2** with calf thymus DNA in Tris buffer was studied by electronic absorption titration, luminescence titration, cyclic voltammetry, circular dichroism, and viscometric measurements. The emission quenching of these complexes by $[Fe(CN)_6]^{4-}$ depressed greatly when bound to DNA. Observed changes in the circular dichoric spectra of DNA in presence of **1** and **2** support the strong binding of complexes with DNA. The relative specific viscosity of DNA bound to **1** and **2** decreased, indicating that the complexes bind to DNA via covalent binding. The results reveal that the extent of DNA binding of **1** was greater than that of **2**. To evaluate the mechanistic pathway of DNA inhibition, counting experiments and MTT assay were employed to assess the induction of apoptosis by **1**. Western blot analysis of whole cell lysates and mitochondrial fractions with Bcl-2 and p-53 family proteins and caspase-3 colorimetry assay were also carried out on a human neuroblastoma cell line SY5Y.

## Introduction

Metal-based pharmaceuticals emerging from interface of inorganic chemistry and biology have witnessed spectacular successes, most notably cisplatin—the archetypal inorganic drug.[1] Although a large number of patients have been cured after cisplatin treatment of cancer, the facts are that the precise mechanism of action remains elusive and that severe side effects develop after administration of the treatment, which has opened up research areas for developing new metal-based anticancer drugs with maximal curative potential and minimal side effects[2] for cancer phenotype (cancers are derived from numerous tissues with new multiple etiologies).

Design of these metal-based pharmaceuticals depends on the ligand framework, the choice of metal ion, and its oxidation state.[3] Ligands can significantly alter the biological properties by modifying reactivity or substitution inertness. Tailored, multifunctional ligands introduced into the metal-based medicinal agents limit the adverse effects of metal ion overload, inhibit selected metalloenzymes, and facilitate metal ion re-distribution.[4] Furthermore, the introduction of chirality (viz. L-amino acids) additionally enhances the pharmacological behavior of the metal complexes by adopting specific conformation and target selective binding affinity[5] as DNA itself exists in nature only in one chiral form.[6] Thus, chiral metal complexes

* Author to whom correspondence should be addressed. E-mail: farukh_arjmand@yahoo.co.in.
[†] Aligarh Muslim University.
[‡] National Institute of Immunology.

(1) Thompson, K. H.; Orvig, C. *Dalton Trans.* **2006**, 761−764.
(2) (a) Reedijk, J. *Chem. Commun.* **1996**, 801−806. (b) Reedijk, J.; Teuben, J. M. In *Cisplatin, Chemistry and Biochemistry of a Leading Anticancer Drug*; Lippard, B., Ed.: Wiley: Weinheim, Germany, 1996; pp 339−362.
(3) (a) Thompson, K. H.; Orvig, C. *Science* **2003**, *300*, 936−939. (b) Reedijk, J. *Proc. Natl. Acad. Sci. U.S.A.* **2003**, *7*, 3611−3616.
(4) Storr, T.; Thompson, K. H.; Orvig, C. *Chem. Soc. Rev.* **2006**, *35*, 534−544.
(5) (a) Stinson, S. C. *Chem. Eng. News* **2001**, *79* (20), 45. (b) Xiaogang, Q.; Trent, J. O.; Fokt, I.; Priebe, W.; Chaires, J. B. *Proc. Natl. Acad. Sci. U.S.A.* **2000**, *97*, 12032−12037.



10.1021/ic061753a CCC: $37.00 
Published on Web 03/23/2007

have a promising future as robust chemotherapeutic agents in medicinal inorganic chemistry.

Copper has been used since antiquity in metal-based therapies.[7] Copper—a bioessential element—plays a key role in biological processes,[8] and its complexes are preferred molecules for cancer inhibition.[9] It has been demonstrated that copper accumulates in tumors due to the selective permeability of cancer cell membranes to copper compounds.[10] Thus, a number of copper complexes have been screened for anticancer activity, and some of them were found to be active both in vitro and in vivo.[11] Literature supports that $Cu^{II}$ ions specifically bind to the N-7 guanine residue of DNA and cause strand breakage.[12] The kinetic analysis of copper DNA interaction and its site-specific binding in DNA have been well-documented.[13] On the contrary, $Sn^{IV}$ complexes prefer to bind to the phosphate backbone of the DNA helix ($Sn^{IV}$ ions have a hard Lewis acid nature, neutralize the negative charge of phosphate sugar, and bring conformational changes in DNA).[14] Thus, bimetallic complexes containing $Cu^{II}$ and $Sn^{IV}$ ions enhance the chemotherapeutic action many-fold as they provide a dual mode of binding at the molecular target site and also exhibit novelty due to preferential selectivity inside the cells.[15] Previous studies of $Cu^{II}$ and $Cu^{II}-Sn^{IV}$ complexes have shown interesting results against various cancerous cell lines (HeLa cells, T47D, HT29).[16] It has been demonstrated that these complexes induce apoptosis via mitochondrial pathway.

In this paper, we report the DNA binding studies of copper complexes by various spectroscopic methods. Complex **1**, which exhibits high binding affinity under physiological condition, is a suitable candidate to be investigated against cancer cells. Thus, in vitro antitumor studies of **1** have been carried out on human neuroblastoma cancer cells (SY5Y).

## Experimental Section

**Materials.** All reagents were of the best commercial grade and were used without further purification. 1,2-Diaminobenzene, $CuCl_2 \cdot 2H_2O$, Tris base (E. Merck), $ZnCl_2$ (Ranbaxy), $SnCl_4$, $ZrCl_4$ (Lancaster), and L-tryptophan (Loba Chemei) were used as received. Disodium salt of calf thymus DNA purchased from Sigma Chemical Company was stored at 4 °C.

**Methods and Instrumentation.** Carbon, hydrogen, and nitrogen contents were determined using a Carlo Erba Analyzer model 1108. Molar conductances were measured at room temperature on a Digsun Electronic conductivity bridge. Fourier-transform infrared (FTIR) spectra were recorded on an Interspec 2020 FTIR spectrometer in Nujol mull. UV−vis spectra were recorded on a USB 2000 Ocean Optics spectrometer in DMSO, and the data were reported as $\lambda_{max}$/nm. The EPR spectra of the copper complexes were acquired on a Varian E 112 spectrometer using X-band frequency (9.1GHz) at liquid nitrogen temperature in solid and solution state. The $^1H$ and $^{13}C$ NMR spectra were obtained on a Bruker DRX-300 spectrometer, and $^{119}Sn$ NMR was recorded on a VXR-300 Varian spectrometer operating at room temperature. Optical rotations of chiral complexes were determined on a Polarimeter Rudolf Autopol III at 25 °C using the sodium D line in EtOH. ESI-MS spectra were recorded on Micromass Quattro II triple quadrupole mass spectrometer. Copper and zinc content were determined on a GBC 932 Plus atomic absorption spectrophotometer.

DNA binding experiments that include absorption spectral traces, luminescence, circular dichoric experiments, viscosity measurements, and cyclic voltammetry conformed to the standard methods[17] and practices previously adopted by our laboratory.[18]

**Evaluation of In Vitro Antitumor Activity.** Stock solution of **1** (1 mg/mL) was prepared in EtOH, stored at room temperature, and diluted suitably with corresponding medium to the required concentrations for all the experiments.

**Cell Culture.** SH-SY5Y cells were obtained from the American Type Culture. Collection was maintained in Dulbecco's modified Eagle medium (DMEM) with high glucose, supplemented with 10% freshly inactivated fetal bovine serum, 1% antibiotic−antimycotics, 1% non-essential amino acid, and 2.5% L-glutamine (all from Life Technologies, Inc.). Rat pheochromocytoma cancer cells (PC-12) cells were cultured in DMEM with high glucose, supplemented with 10% fetal horse serum, 5% FCS, and 1% antibiotic−antimycotics. Both the cell cultures were grown in a humidified incubator at 37 °C with 5% $CO_2$. The medium was replaced after 3 days, and cells were split before they reached confluence. Cells were discarded after about 15 passages.

**Cell Counting.** The cells (SY5Y, PC-12) were plated in a 24-well plate at a density of $2.5 \cdot 10^5$ cells per well in ca. 800 $\mu$L of


(6) (a) Chaires, J. B. *Curr. Med. Chem.* **2000**, *7*, 1−1. (b) Jenkins, T. C. *Curr. Med. Chem.* **2000**, *7*, 99−115. (c) Hegstrom, R. A.; Kondipudi, D. K. *Sci. Am.* **1990**, 108−115.

(7) (a) Scarpellini, M.; Neves, A.; Horner, R.; Bortoluzzi, A. J.; Szpoganics, C.; Zucco, C.; Nome Silva, R. A.; Drago, V.; Mangrich, A. S.; Ortiz, W. A.; Passos, W. A.; Oliveira, M. C.; Terenzi, H. *Inorg. Chem.* **2003**, *42*, 8353−8365. (b) Dhar, S.; Senapati, D.; Das, P. K.; Chattopadhyay, P.; Nethaji, M.; Chakravarty, A. R. *J. Am. Chem. Soc.* **2003**, *125*, 12118−12124.

(8) Crouch, R. K.; Kensler, T. W.; Oberley, L. W.; Sorenson, J. R. J. In *Possible Medicinal Uses of Copper Complexes: Biological and Inorganic Copper Chemistry*; Karlin, K. D., Zubieta, J., Ed.; Adenine Press: New York, 1986.

(9) (a) Vaidyanathan, V. G.; Nair, B. U. *J. Inorg. Biochem.* **2003**, *93*, 271−276. (b) Silvestri, A.; Barone, G.; Ruisi, G.; Giudice, M. T.; Tumminello, S. *J. Inorg. Biochem.* **2004**, *98*, 589−594. (d) Ren, R.; Yang, P.; Zheng, W.; Hua, Z. *Inorg. Chem.* **2000**, *39*, 5454−5463.

(10) Apelgot, S.; Coopy, J.; Fromentin, A.; Guille, E.; Poupon, M. F.; Roussel, A. *Anticancer Res.* **1986**, *6*, 159.

(11) (a) Fernandes, C.; Parrilha, G. L.; Lessa, J. A.; Santiago, L. J. M.; Kanashiro, M. M.; Boniolo, F. S.; Bortoluzzi, A. J.; Vugman, N. V.; Herbst, M. H.; Horn, A., Jr. *Inorg. Chim. Acta* **2006**, *359*, 3167−3176. (b) Bales, B. C.; Kodama, T.; Weledji, Y. N.; Pitie, M.; Meunier, B.; Greenberg, M. M. *Nucleic Acid Res.* **2005**, *33*, 5371−5379.

(12) (a) Ito, T.; Thyagarajan, S.; Karlin, K. D.; Rokita, S. E. *Chem. Commun.* **2005**, 4812−4814. (b) Chikira, M.; Tomizawa, Y.; Sugizaki, T.; Sugawara, N.; Yamazaki, T.; Sasano, A.; Shindo, H.; Palaniandavar, M.; Antholine, W. E. *J. Inorg. Biochem.* **2002**, *89*, 163−173.

(13) (a) Zhang, Q.; Zhang, F.; Wang, W.; Wang, X. *J. Inorg. Biochem.* **2006**, *100*, 1344−1352. (b) Chakravarty, A. R.; Reddy, P. A. N.; Santra, B.; Thomas, A. M. *Proc. Indian Acad. Sci.* **2002**, *114*, 391−401.

(14) (a) Zelder, F. H.; Mokhir, A. A.; Kramer, R. *Inorg. Chem.* **2003**, *42*, 8618−8620. (b) Hoti, N.; Ma, J.; Tabassum, S.; Wang, Y.; Wu, M. *J. Biochem.* **2003**, *134*, 521−528.

(15) (a) Hoti, N.; Zhu, D.; Song, Song, Z.; Wu, Z.; Tabassum, S.; Wu, M. *J. Pharmacol. Exp. Ther.* **2004**, *311*, 22−33. (b) Chauhan, M.; Arjmand, F. *Transition Met. Chem.* **2005**, *30*, 481−487.

(16) (a)Bolos, C. A.; Papazisis, K. T.; Kortsaris, A. H.; Voyatzi, S.; Zambouli, D.; Kyriakidis, D. A. *J. Inorg. Biochem.* **2002**, *88*, 25−36. (b) Chaviara, A. T.; Cox, P. J.; Repana, K. H.; Papi, R. M.; Papazisis, K. T.; Zambouli, D.; Kortsaris, A. H.; Kyriakidis, D. A.; Bolos, C. A. *J. Inorg. Biochem.* **2004**, *98*, 1271−1283.

(17) (a) Marmur, J. *J. Mol. Biol.* **1961**, *3*, 208−214. (b) Reicmann, M. E.; Rice, S. A.; Thomas, C. A.; Doty, P. *J. Am. Chem. Soc.* **1954**, *76*, 3047−3053. (c) Wolfe, A.; Shimer, G. H.; Meehan, T. *Biochemistry* **1987**, *26*, 6392−6396. (d) Lakowiez, J. R.; Webber, G. *Biochemistry* **1973**, *12*, 4161−4170. (e) Cohen, G.; Eisenberg, H. *Biopolymers* **1969**, *8*, 45−55. (f) Eriksson, M.; Leijon, M.; Hiort, C.; Norden, B.; Graslund, A. *Biochemistry* **1994**, *33*, 5031−5040.

(18) (a) Arjmand, F.; Chauhan, M. *Helv. Chim. Acta* **2005**, *88*, 2413−2423. (b) Chauhan, M.; Arjmand, F. *Chem. Biodiv.* **2006**, *3*, 660−676.

medium and kept in the incubator for 24 h. The cells were then serum starved for ca. 12 h and treated with various doses (2, 4, 6, and 8 $\mu$L) of **1** in duplicates. No treatment was given to the control sets. After 24 h of treatment, the medium was removed, and the cells were washed with phosphate-buffered saline (PBS) (400 $\mu$L). In order to detach cells, the wells were trypsinized with 50 $\mu$L of trypsin in the case of SY5Y cells. The cell mortality was evaluated by counting the cells using a hemocytometer. The data were presented by plotting a graph between the percentage of live cells and compound concentration.

**3-(4,5-Dimethylthiazol-2-yl)-2,5-diphenyl-2*H*-tetrazolium Bromide (MTT) Assay.** The cytotoxicity exerted by **1** was assessed by the MTT assay. The assay is based on the fact that only live cells reduce yellow MTT but not dead cells to blue formazan products. Briefly, $7 \cdot 10^4$ tumor cells (SY5Y) were plated in a 96-well flat bottom microtiter plates in 150 $\mu$L of corresponding medium. Cells were incubated for 24 h to adhere properly. The cells were treated with **1** in different concentrations and incubated for 24 h. Untreated cells were used as negative control, since **1** is EtOH-soluble so the cells treated with EtOH without **1** were used as controls. MTT (15 $\mu$L) was added to each well to a final concentration of 5 mg/mL and incubated additionally for 3 h at 37 °C. The reaction was terminated by removing the medium; the formazan dye was dissolved by adding 50 $\mu$L of 0.1 N HCl in 2-propanol. The plates were read at 570 and 655 nm on a Bio-Rad 680-microplate reader. The assay was performed in triplicate, and the arithmetic means were determined by using Excel software. The results were expressed as the percentage of alive cells versus [complex **1**] as calculated from MTT reduction, assuming that the absorbance of the negative controls was 100%.

**Preparation of Whole Cell Lysates.** To prepare the whole cell lysates, cells were first grown in 6 cm dishes. After treatment with **1**, cells were harvested at different time points. Cells were washed with PBS, pH 7.2, and lysed with 500 $\mu$L of lysis buffer (10 mM Tris, 150 mM NaCl, 1% Triton X-100, 5 mM EDTA, 25 mM glycerophosphate, 1 mM phenylmethylsulfonyl fluoride, 2 mM, benzamidine, 10 mg/mL aprotinin, 10 mg/mL leupeptin, and 1 mM sodium orthovanadate) and incubated on ice for 15 min. The lysed cells were transferred to 1.5 mL Eppendorf tubes and were centrifuged at 16 000 rpm for 20 min at 4 °C. Supernatant was collected, and Pierce bicinchoninic acid (BCA) protein assay reagent was used to determine the protein concentration. The aliquots of cell lysates were boiled with sodium dodecyl sulfate (SDS) sample buffer and analyzed by Western blot using the indicated antibodies.

**Preparation of Mitochondrial Lysates.** To prepare the mitochondrial lysates, cells were first grown in 6 cm dishes. After treatment with **1**, cells were harvested at different time points. Cells were washed twice with ice-cold sterile PBS (pH 7.2), and cell pellets were resuspended in RSB buffer (a hypotonic buffer) (10 mM NaCl, 1.5 mM $MgCl_2$, 10 mM Tris-HCl, pH 7.5) for 10 min to allow cells to swell. The swollen cells were break opened by several strokes of pestle of Dounce homogenizer; 2.5× MS buffer (an iso-osmotic buffer) (525 mM mannitol, 175 mM sucrose, 12.5 mM Tris-HCl, pH 7.5, 2.5 mM EDTA, pH 7.5) was added immediately to it and mixed well by inverting the homogenizer a couple of times. The homogenate was transferred to a centrifuge tube for differential centrifugation, and then 1× MS buffer (210 mM mannitol, 70 mM sucrose, 5 mM Tris-HCl, pH 7.5, 1 mM EDTA, pH 7.5) was added. The mitochondrial extracts for the detection of Bcl-2 family proteins (Bad,and Bak) were fractionated onto 12% polyacrylamide gel. Proteins were visualized by enhanced chemiluminescence.

**Western Blot Analysis.** Cell lysates containing a total protein of 20−30 $\mu$g were loaded onto 12% SDS−polyacrylamide gels. Resolved proteins were then electrophoretically transferred onto a polyvinylidene fluoride membrane. The blot was blocked with 5% skim milk in 0.1% Tween 20 Tris-buffered saline (TBS) solution for 2 h at room temperature; all antibody binding reactions were performed in the same buffer. The membrane was incubated at 4 °C overnight with primary antibodies. After being washed, the membrane was then incubated with activator protein-conjugated secondary antibody for 1 h at room temperature and washed again in TBS/Tween 20. The signal was detected by the enhanced chemiluminescence Western blot system (Pierce).

**Caspase Activation and Activity Assay.** The caspase activity assay was based on spectrophotometric detection of the chromatophore *p*-nitroanilide (pNA) after cleavage from the labeled substrate DEVD-pNA by caspase-3 like proteases. Cultured SY5Y cells were treated with and without **1** (2.0 $\mu$L/mL) for 0−18 h at 37 °C. Cells were lysed, and assay was performed with the Caspase-3/CPP32 colorimetric kit (BioVision) according to the manufacturer's protocol.

**Synthesis of [Bis(1,2-diaminobenzene)copper/zinc(II)] Chloride.** To a solution of $CuCl_2.2H_2O$ (1.71 g, 10 mmol) in 30 mL of MeOH was added a methanolic solution of 1,2 diaminobenzene (2.16 g, 20 mmol) in 1:2 molar ratio. The mixture was stirred for 15 min. The dark green product obtained was washed with $Et_2O$ and dried in vacuo. [Bis(1,2-diaminobenzene) zinc(II)] chloride was also synthesized by a similar procedure with $ZnCl_2$.

**Synthesis of $C_{23}H_{31}N_6O_6CuSn_2Cl_5$ (1).** [Bis(1,2-diaminobenzene) copper(II)] chloride (3.49 g, 10 mmol) dissolved in 20 mL of MeOH was treated with $SnCl_4$ (2.34 mL in $CCl_4$, 20 mmol) in 1:2 molar ratio. The green colored solution turned to red, and the volume of the resulting solution was reduced to 10 mL by rotary evaporator. A methanolic solution of L-tryptophan (2.04 g, 10 mmol) was added to the above reaction mixture and refluxed for 72 h. The solvent was further removed by rotary evaporator to give a dark brown colored solid product, which was filtered, washed with hexane, and dried in vacuo. Yield: 4 g, 51.0%. mp 240 °C, $[\alpha]_D$ (EtOH) +26. Anal. Calcd. for $C_{23}H_{31}N_6O_6CuSn_2Cl_5$: C, 28.57; H, 3.20; N, 8.63. Found: C, 28.45; H, 3.11; N, 8.54. Atomic absorption for $Cu^{II}$, in ppm: Calcd. 0.755. Found: 0.753. Selected IR data in Nujol ($\nu$/cm$^{-1}$): 1616 (sym COO); 1383 (antisym COO); 3185 $\nu$ (N−H); 1528 $\delta$ (N−H); 749 (Ar); 1239 (imidazole N−H); 3386 ($NH_2 + H_2O$); 460 (Cu−N); 520 (Cu−O); 448 (Sn−N); 330 (Sn−Cl). Molar conductance: $\wedge_M$ ($1 \cdot 10^{-3}$ M, EtOH): 40.0 $\Omega^{-1} \cdot cm^2 \cdot mol^{-1}$ (1:1 electrolyte). UV−vis ($1 \cdot 10^{-4}$ M, MeOH) $\lambda_{max}$/nm 257; 410; 620. ESI ($m/z^+$): 930.5 $[C_{23}H_{31}N_6O_6CuSn_2Cl_4]^+$.

**Synthesis of $C_{23}H_{31}N_6O_6CuZr_2Cl_5$ (2).** This complex was prepared by adopting the procedure given for **1** by using $ZrCl_4$ (4.66 g, 20 mmol). Yield: 4.7 g (46%) mp 200 °C, $[\alpha]_D$ (EtOH) +12. Anal. Calcd. for $C_{23}H_{31}N_6O_6CuZr_2Cl_5$: C, 30.30; H, 3.40; N, 9.22. Found: C, 30.25; H, 3.35; N, 9.18. Atomic absorption for $Cu^{II}$, in ppm: Calcd. 0.756. Found: 0.750. Selected IR data on Nujol ($\nu$/cm$^{-1}$): 1622 (sym COO); 1390 (antisym COO); 3190 $\nu$ (N−H); 1535 $\delta$ (N−H); 755 (Ar); 1242 (imidazole N−H); 3380 ($NH_2 + H_2O$); 465 (Cu−N); 525 (Cu−O); 450 (Zr−N); 337 (Zr−Cl). Molar conductance: $\wedge_M$ ($1 \cdot 10^{-3}$ M, EtOH): 43.0 $\Omega^{-1} \cdot cm^2 \cdot mol^{-1}$ (1:1 electrolyte). UV−vis ($1 \cdot 10^{-4}$ M, MeOH) $\lambda_{max}$/nm 262; 420; 630. ESI ($m/z^+$): 874.9 $[C_{23}H_{31}N_6O_6CuZr_2Cl_4]^+$.

**Synthesis of $C_{23}H_{31}N_6O_6ZnSn_2Cl_5$ (3).** This complex was synthesized according to procedure described for **1** with [bis(1,2-diaminobenzene) zinc(II)] chloride (3.51 g, 10 mmol). Blackish-brown colored product was isolated. Yield 4.9 g, 62%. mp 125 °C, $[\alpha]_D$ (EtOH) +17. Anal. Calcd. for $C_{23}H_{31}N_6O_6ZnSn_2Cl_5$: C, 28.53;

**Scheme 1**

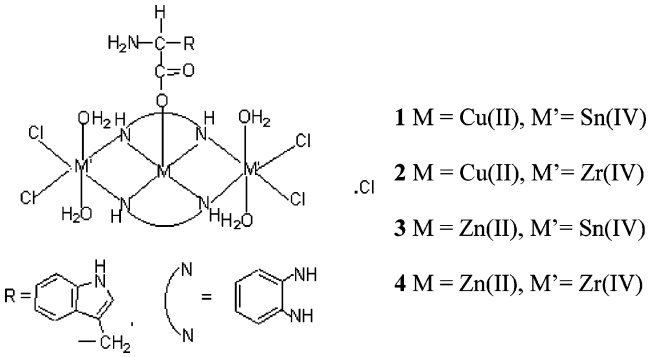

**1** M = Cu(II), M'= Sn(IV)

**2** M = Cu(II), M'= Zr(IV)

**3** M = Zn(II), M'= Sn(IV)

**4** M = Zn(II), M'= Zr(IV)

H, 3.20; N, 8.67. Found: C, 28.45; H, 3.21; N, 8.59. Atomic absorption for $Zn^{II}$, in ppm: Calcd. 0.780. Found: 0.778. Selected IR data on Nujol ($\nu$/cm$^{-1}$): 1620 (sym COO); 1387 (antisym COO); 3187 $\nu$ (N−H); 1530 $\delta$ (N−H); 751 (Ar); 1240 (imidazole N−H); 3385 ($NH_2$ + $H_2O$); 462 (Zn−N); 522 (Zn−O); 444 (Sn−N); 339 (Sn−Cl). Molar conductance: $\Lambda_M$ ($1\cdot10^{-3}$ M, EtOH): 42.0 $\Omega^{-1}\cdot cm^2\cdot mol^{-1}$ (1:1 electrolyte). UV−vis ($1\cdot10^{-4}$ M, MeOH) $\lambda_{max}$/nm = 277; 390. $^1$H NMR (300 MHz, DMSO-$d_6$, $\delta$): 5.3 ($NH_2$); 4.3 (C−H); 3.3 ($CH_2$); 7.1 (HC═C); 6.9 (imidazole N−H); 7.4−7.7 (ArH). $^{13}$C NMR (75.44 MHz, DMSO-$d_6$, $\delta$): 173 (O−C═O); 56 (C−H); 38 ($CH_2$); 114 (NH−CH); 120−132 (Ar−C). $^{119}$Sn NMR (149 MHz, DMSO-$d_6$, $\delta$): −625; −668. ESI ($m/z^+$): 932.3 $[C_{23}H_{31}N_6O_6ZnSn_2Cl_4]^+$.

**Synthesis of $C_{23}H_{31}N_6O_6ZnZr_2Cl_5$ (4).** This complex was synthesized with $ZrCl_4$ (4.66 g, 20 mmol) and [bis(1,2-diaminobenzene) zinc] chloride (3.51 g, 10 mmol) by a procedure similar to that described for **1**. Yield 5.2 g, 51%. mp 150 °C, $[\alpha]_D$ (EtOH) +72. Anal. Calcd. for $C_{23}H_{31}N_6O_6ZnZr_2Cl_5$: C, 30.20; H, 3.39; N, 9.20. Found: C, 30.15; H, 3.36; N, 9.18. Atomic absorption for $Zn^{II}$, in ppm: Calcd. 0.780. Found: 0.776. Selected IR data on Nujol ($\nu$/cm$^{-1}$): 1619 (sym COO); 1390 (antisym COO); 3190 $\nu$ (N−H); 1539 $\delta$ (N−H); 752 (Ar); 1245 (imidazole N−H); 3384 ($NH_2$ + $H_2O$); 462 (Zn−N); 526 (Zn−O); 445 (Zr−N); 335 (Zr−Cl). Molar conductance: $\Lambda_M$ ($1\cdot10^{-3}$ M, EtOH): 45.0 $\Omega^{-1}\cdot cm^2\cdot mol^{-1}$ (1:1 electrolyte). UV−vis ($1\cdot10^{-4}$ M, MeOH) $\lambda_{max}$/nm 270; 400. $^1$H NMR (300 MHz, DMSO-$d_6$, $\delta$): 5.4 ($NH_2$); 4.2 (C−H); 3.4 ($CH_2$); 7.1 (HC═C); 6.9 (imidazole N−H); 7.4−7.7 (ArH). $^{13}$C NMR (75.44 MHz, DMSO-$d_6$, $\delta$): 174 (O−C═O); 56 (C−H); 37 ($CH_2$); 116 (NH−CH); 120−132 (ArC). ESI ($m/z^+$): 876.7 $[C_{23}H_{31}N_6O_6ZnZr_2Cl_4]^+$.

## Results and Discussion

Syntheses of trinuclear complexes **1**−**4** were achieved by mixing stoichiometric amounts of [bis(1,2-diaminobenzene) copper(II)/zinc(II)] chloride and $SnCl_4$/$ZrCl_4$ followed by reaction with L-tryptophan as chiral auxiliary (Scheme 1). The complexes are stable toward air and moisture and soluble in EtOH, DMSO, and DMF. Molar conductance values of complexes in EtOH ($1\cdot10^{-3}$ M) at 25 °C suggest their 1:1 electrolytic nature (40−45 $\Omega^{-1}\cdot cm^2\cdot mol^{-1}$). Due to the presence of chiral auxiliary L-tryptophan, **1**−**4** exhibited optical rotation $[\alpha]_D$ values of +26, +12, +17, and +72, respectively, which indicate that all the complexes are optically active. In **1**−**4**, the coordination geometry of central metal ion ($Cu^{II}$, $Zn^{II}$) is square pyramidal; Sn/Zr is present in hexacoordinated environment, which is proposed on the basis of spectroscopic studies. DNA binding studies were carried out with copper complexes **1** and **2**, and their analogous zinc complexes **3** and **4** were synthesized only for NMR studies. The interaction studies of **1** and **2** with calf thymus (CT)-DNA indicate that **1** binds to DNA with a strong affinity. Thus, the in vitro antitumor activity was performed with **1**.

**IR Spectroscopy.** The bands around 1660 and 1430 cm$^{-1}$ observed in the free amino acid assigned to antisymmetric and symmetric O−C═O stretching vibrations were shifted to lower frequencies, suggesting the terminal coordination mode of carboxylate group of the L-tryptophan to the transition metal ion via deprotonation.[19] The bands in the 3183−3190 cm$^{-1}$ region and the 1528−1540 cm$^{-1}$ region were assigned to $\nu$(NH) and $\delta$(NH), respectively, suggesting that $NH_2$ groups of 1,2-diaminobenzene are coordinated to copper/zinc and simultaneously to tin/zirconium metal ions by the elimination of HCl molecules.[20] The IR spectra of **1**−**4** exhibited a very broad band at ∼3386 cm$^{-1}$ corresponding to the uncoordinated amino group of L-tryptophan, suggesting that the amino acid binds to the metal ion in monodentate fashion. As a consequence of the presence of a water molecule coordinated to a tin/zirconium metal ion, the IR spectra of the complexes also displays a band in 3300−3400 cm$^{-1}$ region.[21] Thus, the individual assignment of the coordinated water molecule and free $NH_2$ group of L-tryptophan was difficult. However, the presence of a free $NH_2$ group of tryptophan moiety was further substantiated by $^1$H NMR spectra of zinc complexes **3** and **4**. The coordination of water molecules to the Sn/Zr metal ion was supported by the appearance of non-ligand band in the region 840−851 cm$^{-1}$ attributed to rocking mode of water.[22] Other medium intensity bands at the 749−755 cm$^{-1}$ signature of aromatic ring vibrations and at 1239−1245 cm$^{-1}$ due to imidazole−NH were also observed. The coordination of L-tryptophan and complex formation were also revealed by the presence of medium intensity (Cu/Zn−N), (Cu/Zn−O), (Sn/Zr−N), and (Sn/Zr−Cl) bands around ∼460, ∼520, ∼448, and ∼330 cm$^{-1}$, respectively, in the far-IR region.[23]

**NMR Spectroscopy. 3** and **4** were characterized by $^1$H, $^{13}$C, 2D COSY, and $^{119}$Sn NMR spectra recorded in DMSO-$d_6$ solution and showed signals for aliphatic and aromatic protons with chemical shift values in accordance with the proposed structure. Apart from the absence of signal at 10.0−12.0 ppm due to the deprotonation of the carboxylic acid group of L-tryptophan, the $^1$H NMR spectra of complexes also exhibited the signals of a $NH_2$ group of amino acid at ∼5.3 ppm, indicating the coordination of amino acid in a unidentate manner to the zinc atom.[24] Coupled with these

(19) Yang C. T.; Moubaraki, B.; Murray, K. S.; Vittal, J. J. *Dalton Trans.* **2003**, 880−889.
(20) Sousa, G. F. de; Deflon, V. M.; Gambardella, M. T. P.; Francisco, R. H. P. *Inorg. Chem.* **2006**, *45*, 4518−4525.
(21) Szorsik, A.; Nagy, L.; Pellerito, L.; Yamaguchi, T.; Yoshida, K. *J. Radioanal. Nucl. Chem.* **2003**, *256*, 3−10.
(22) Reddy, P. R.; Reddy, A. M. *Indian J. Chem.* **2002**, *41A*, 2083−2087.
(23) (a) Ma, C.; Han, Y.; Zhang, R.; Wang, D. *Dalton Trans.* **2004**, 1832−1840. (b) Bolos, C. A.; Niokolov, G. St.; Ekateriniadou, L.; Kortsaris, A.; Kyriakadis, D. A. *Met.-Based Drugs* **1998**, *5*, 323−332.
(24) (a) Kemp, W. *Organic Spectroscopy*, 3rd ed.; W. H. Freeman: New York, 1991. (b) Ather, F.; Arjmand, F.; Tabassum, S. *Transition Met. Chem.* **2001**, *26*, 426−429.

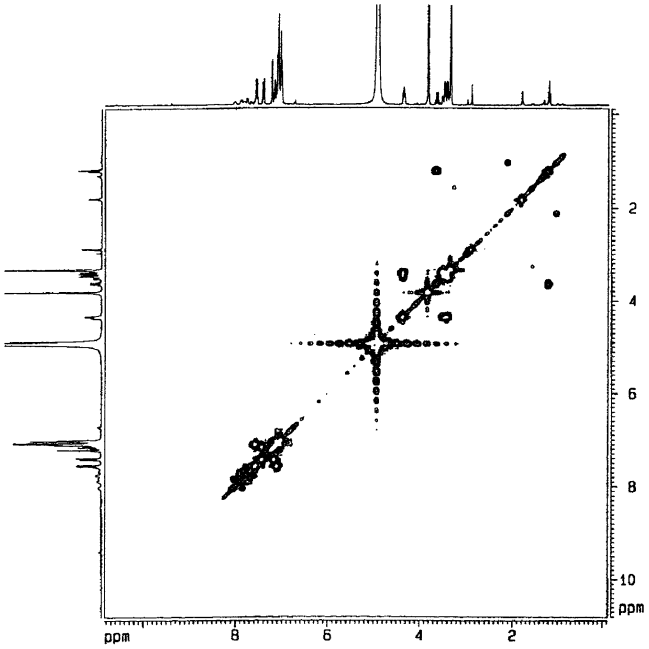


**Figure 1.** $^{1}H-^{1}H$ 2D cosy NMR spectrum of complex **3**.

observations, the characteristic signals at 4.3, 3.3, 6.9, and 7.1 ppm corresponding to asymmetric CH, $CH_2$, imodazole NH, and CH═C groups, respectively, further confirmed the presence of L-tryptophan moiety in chiral metal complexes **3** and **4**.[24,25] The resonance at ~7.3 ppm arises due to the -NH proton of 1,2-diaminobenzene.[26] This feature is commensurate with the fact that the amino group of 1,2-diaminobenzene was coordinated to the Sn/Zr metal ion through monodeprotonation and simultaneously to the zinc metal atom. The assignments of the proton signals were also obtained from 2D COSY NMR, which exhibits relatively the same resonances observed in $^{1}H$ NMR spectra of **3** and **4** (Figure 1).

The $^{13}C$ NMR spectra of **3** and **4** were characterized by various resonances due to O—C═O, chiral CH, $CH_2$, and N—CH carbons at 173, 56, 38.0, and 114 ppm, respectively, of the coordinated L-tryptophan. In addition, $^{13}C$ NMR spectra of **3** and **4** reveal aromatic carbons at 120−132 ppm.

$^{119}Sn$ NMR spectroscopy has been found to be a useful technique for structure elucidation and the nature of coordination of tin atom in complexes. The $^{119}Sn$ chemical shift, $\delta(^{119}Sn)$, is sensitive to the chemical environments of the tin atom. $^{119}Sn$ NMR spectrum of **3** displayed two signals at −625 and −668 ppm, due to the presence of two tin metal centers. These chemical shifts values are consistent with those reported for complexes with the hexacoordinated geometry of a tin metal atom.[27]

**Absorption Spectroscopy.** The UV−vis spectra of **1** and **2** at room temperature in DMSO exhibited broad and intense absorption maxima centered at 620 and 630 nm, respectively.[28] In addition, metal to ligand charge-transfer transition was observed at 410 and 420 nm, respectively.[29] This spectral feature is typical of pentacoordinated copper complexes with distorted square pyramidal geometry, which generally exhibited a band in the 550−660 nm region ($d_{xz}$, $d_{yz} \rightarrow d_{x^2-y^2}$).[30] The absorption spectra of **3** and **4** revealed one intense band around 400 nm, which corresponds to the metal to ligand charge-transfer transitions.[31] All the complexes displayed strong band in the UV region at 257−277 nm attributed to $\pi - \pi^*$ transition.[32]

**EPR Spectra.** The X-band EPR spectra of **1** and **2** were acquired at liquid nitrogen temperature under the magnetic field strength 3000 ± 1000 G using tetracyanoethylene as a field marker. In solid state, both complexes show an isotropic band centered at $g = 2.04$.[33] The value was in good agreement with the unpaired electron mainly located in the $d_z^2$ orbital. This pattern is typical for copper complexes with square pyramidal environment. The geometry of the complexes in solution state was confirmed by running the spectra in DMSO. The solution EPR spectra of **1** and **2** at LNT were also well-reproduced and exhibited only a single isotropic signal at $g = 2.09$ and 2.07, respectively.[34] This is consistent with the square pyramidal geometry of copper ion as well as with the results of solid-state EPR spectra.

**DNA Binding Studies.** Since DNA is the primary pharmacological target of many antitumor compounds[35] DNA−metal complex interaction has paramount importance in understanding the mechanism of tumor inhibtion for the treatment of cancer. The interaction of **1** and **2** with DNA were analyzed by a number of techniques, such as absorption titration, cyclic voltammetry, fluorescence spectroscopy, circular dichroism, and viscosity measurements.

**Absorption Titration.** The absorption spectra of **1** and **2** in the absence and presence of CT-DNA (at a constant concentration of complexes, $0.16 \cdot 10^{-4}$ M) are shown in Figure 2. In the UV region, **1** and **2** exhibited intense absorption bands at 257 and 262 nm, respectively, which were assigned to $\pi-\pi^*$ transition of aromatic chromophore and other at ~420 nm in the visible region, which is attributed to metal to ligand charge transfer (MLCT) bands. With increasing CT-DNA ($0-0.4 \cdot 10^{-4}$ M), the absorption bands of **1** and **2** are affected, exhibiting hyperchromism of

(25) Tak, A. A.; Arjmand, F.; Tabassum, S. *Met.-Based Drugs* **2002**, *9*, 81−90.
(26) Aggarwal, P.; Kamboj, R. C.; Gupta, S. C.; Dhawan, S. N. *Indian J. Chem.* **2006**, *45B*, 1322−1324.
(27) Pettinari, C.; Caruso, F.; Zaffaroni, N.; Villa, R.; Marchetti, F.; Pettinari, R.; Phillips, C.; Tanski, J.; Rossi, M. *J. Inorg. Biochem.* **2006**, *100*, 58−69.
(28) (a) Patra, A. K.; Dhar, S.; Nethaji, M.; Chakravarty, A. R. *Dalton Trans* **2005**, 896−902. (b) Horn, A., Jr.; Fernandes, C.; Bortoluzzi, A. J.; Vugman, N. V.; Herbst, M. H. *J. Mol. Struct.* **2005**, *749*, 96.
(29) Tas, E.; Aslanoglu, M.; Ulusoy, M.; Temel, H. *J. Coord. Chem.* **2004**, *57*, 677−684.
(30) Chattopadhyay, S. K.; Seth, S.; Mak, T. C. W. *J. Coord. Chem.* **2002**, *55*, 259−270. McLachlan, G. A.; Fallon, G. D.; Martin, R. E.; Spiccia, L. *Inorg. Chem.* **1995**, *35*, 254−261.
(31) Das, T. M.; Rao, C. P.; Kolehmainen, E.; Kadam, R. M.; Sastry, M. D. *Carbohyr. Res.* **2002**, *337*, 289−296.
(32) Uma, V.; Kanthimathi, M.; Weyhermuller, T.; Nair, B. U. *J. Inorg. Biochem.* **2005**, *99*, 2299−2307.
(33) (a) Kurosaki, H.; Sharma, R. K.; Aoki, S.; Inoue, T.; Okamoto, Y.; Sugiura, Y.; Doi, M.; Ishida, T.; Otsuka, M.; Goto, M. *J. Chem. Soc. Dalton Trans.* **2001**, 441−447. (b) Du, M.; Guo, Y. M.; Bu, X. H.; Ribas, J.; Monfort, M. *New J. Chem.* **2002**, *26*, 939−945.
(34) Colacio, E.; Dominguez-Vera, J. M.; Ghazi, M.; Rivekas, R.; Klinga, M.; Moreno, J. M. *Inorg. Chem.* **1998**, *37*, 3040−3045.
(35) Quiroga, A. G.; Perez, J. M.; Lopez-Solera, I.; Montero, E. I.; Masaguer, J. R.; Alonso, C.; Navarro-Ranninger, C. *J. Inorg. Biochem.* **1998**, *69*, 275−281.

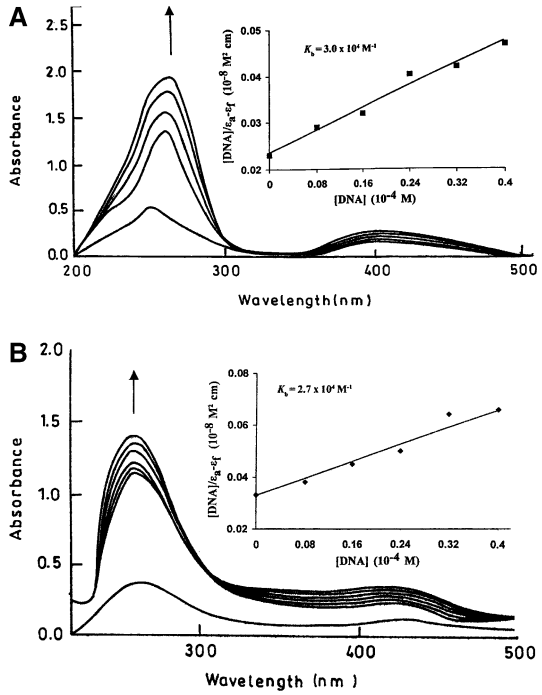


**Figure 2.** Absorption spectral traces of (A) complex **1** and (B) complex **2** in Tris-HCl buffer upon addition of CT-DNA. Inset: Plots of [DNA]/$\epsilon_a - \epsilon_f$ vs [DNA] for the titration of CT-DNA with complexes: ■, experimental data points; —, linear fitting of the data. [complex] $0.16 \cdot 10^{-4}$ M, [DNA] $0-0.4 \cdot 10^{-4}$ M.

26% and 24% and red shift of 6 and 4 nm in $\pi-\pi^*$ transitions of **1** and **2**, respectively, when saturated around [DNA]/[complex] = 25. In addition, the spectral changes in MLCT bands at 410 and 420 nm also reveal hyperchromism, although the extent of hyperchromism is lower than that observed in case of $\pi-\pi^*$. A strong hyperchromic effect with a significant red shift in $\pi-\pi^*$ transition was observed for **1**, suggesting that this complex possess a higher propensity for DNA binding. The extent of hyperchromism was different for **1** and **2**, which could be due to the presence of second metal ion (less reactive $Zr^{IV}$ ion is present in **2** in comparison to $Sn^{IV}$ metal ion in **1**).[36] The experimental results suggest that in both the complexes $Sn^{IV}/Zr^{IV}$ metal ions bind to the phosphate backbone of the DNA helix[37] while the copper(II) ion preferentially attacks at the N-7 position of guanine and shows structural and conformational changes in DNA.[38] Nevertheless, 1,2-diaminobenzene and a side chain of L-tryptophan provide an aromatic moiety to **1** and **2** so the binding of two complexes involving intercalation of an aromatic ring between the base pairs of DNA could not be ruled out.[39]

In order to compare quantitatively the binding strength of **1** and **2** with CT-DNA, the intrinsic binding constants $K_b$ of the complexes were determined with eq 1 by monitoring the changes in absorbance of the $\pi-\pi^*$ bands with increasing concentration of CT-DNA:

$$\frac{[\mathrm{DNA}]}{\epsilon_a - \epsilon_f} = \frac{[\mathrm{DNA}]}{\epsilon_b - \epsilon_f} + \frac{1}{K_b(\epsilon_b - \epsilon_f)} \quad (1)$$

where $\epsilon_a$, $\epsilon_f$, and $\epsilon_b$ correspond to $A_{obsd}/[Cu]$), the extinction coefficient for free copper complex, and the extinction coefficient for the copper complex in the fully bound form, respectively. A plot of [DNA]/($\epsilon_a - \epsilon_f$) versus [DNA], where [DNA] is the concentration of DNA in the base pairs, gives $K_b$ as the ratio of slope to the intercept. The binding constants obtained for **1** and **2** are $3.0 \cdot 10^4$ and $2.7 \cdot 10^4$ $M^{-1}$, respectively. These $K_b$ values suggest that **1** has a strong binding affinity for calf thymus DNA.

**Steady-State Emission Titration.** At room temperature, **2** exhibits strong emission bands around 350 nm with a shoulder when excited at 262 nm while for **1** an excitation wavelength of 257 nm was used and total emission intensity was monitored at 550 nm. Fixed amounts of **1** and **2** were titrated with increasing amounts of DNA, over a range of DNA concentration from 0 to $13 \cdot 10^{-5}$ M. Titration of CT-DNA led to a remarkable decrease in the emission intensity of **1** and **2**, as illustrated in Figure 3, panels A and B, respectively. The relative fluorescence intensity as a function of CT-DNA concentration (in terms of [DNA]/[M]) was plotted in the insets of Figure 3. Complex **1** produced a large reduction in emission intensity in the presence of DNA in comparison to **2**. The quenching of the luminescent excited state of the complexes was due to the energy/electron transfer from the guanine base of DNA to the MLCT of the complexes.[40]

To further demonstrate the interaction pattern of the fluorescence probe **1** and **2** with DNA, we performed the $[Fe(CN)_6]^{4-}$ quenching experiments as $[Fe(CN)_6]^{4-}$ is a dynamic fluorescence quencher and provides a sensitive tool to examine the nature of the interaction of the probe with the DNA.[41] The quenching efficiency is evaluated by the Stern−Volmer constant $K_{sv}$, which varies with the experimental conditions:

$$I_0/I = 1 + K_{sv} r_{Cu} \quad (2)$$

where $I_0$ and $I$ are the emission intensities in the absence and the presence of the complex, respectively. A large value of binding constant corresponds to poorer protection and weaker binding to DNA and vice versa. Figure 4 shows the Stern−Volmer plots with ferrocyanide anion as quencher for **1** and **2**. The plot of free complexes **1** and **2** gave $K_{sv} = 14 \cdot 10^2$ and $8 \cdot 10^2$ $M^{-1}$, respectively. In the presence of DNA, the quenching curve was obviously depressed, reflecting that the complexes were protected by the DNA helix. The $K_{sv}$

(36) Mancin, F.; Scrimin, P.; Tacilla, P.; Tonellato, U. *Chem. Commun.* **2005**, 2540−2548.
(37) (a) Pellerito, L.; Nagy, L. *Coord. Chem. Rev.* **2002**, *224*, 111−150. (b) Janeso, A.; Nagy, L.; Moldrheim E.; Sletten, E. *J. Chem. Soc. Dalton Trans.* **1999**, 1587−1594.
(38) (a) Hirohama, T.; Karunuki, Y.; Ebina, E.; Suzaki, T.; Arii, H.; Chikira, M.; Selvi, P. T.; Palaniandavar, M. *J. Inorg. Biochem.* **2005**, *99*, 1205−1219.
(39) Liu, J.; Lu, T. B.; Deng, H.; Ji, L. N. *Transition Met. Chem.* **2003**, *28*, 116−121.
(40) (a)Liu, F.; Wang, K.; Bai, G.; Zhang, Y.; Gao, L. *Inorg. Chem.* **2004**, *43*, 1799−1806. (b) Wu, J. Z.; Yuan, L.; Wu, J. F. *J. Inorg. Biochem.* **2005**, *99*, 2211−2216.
(41) (a) Midorikawa, K.; Kawanishi, S. *FEBS Lett.* **2001**, *495*, 187−190. (b) Kang, J. H.; Eum, W. S. *Biochim. Biophys. Acta* **2000**, *1524*, 162−170.

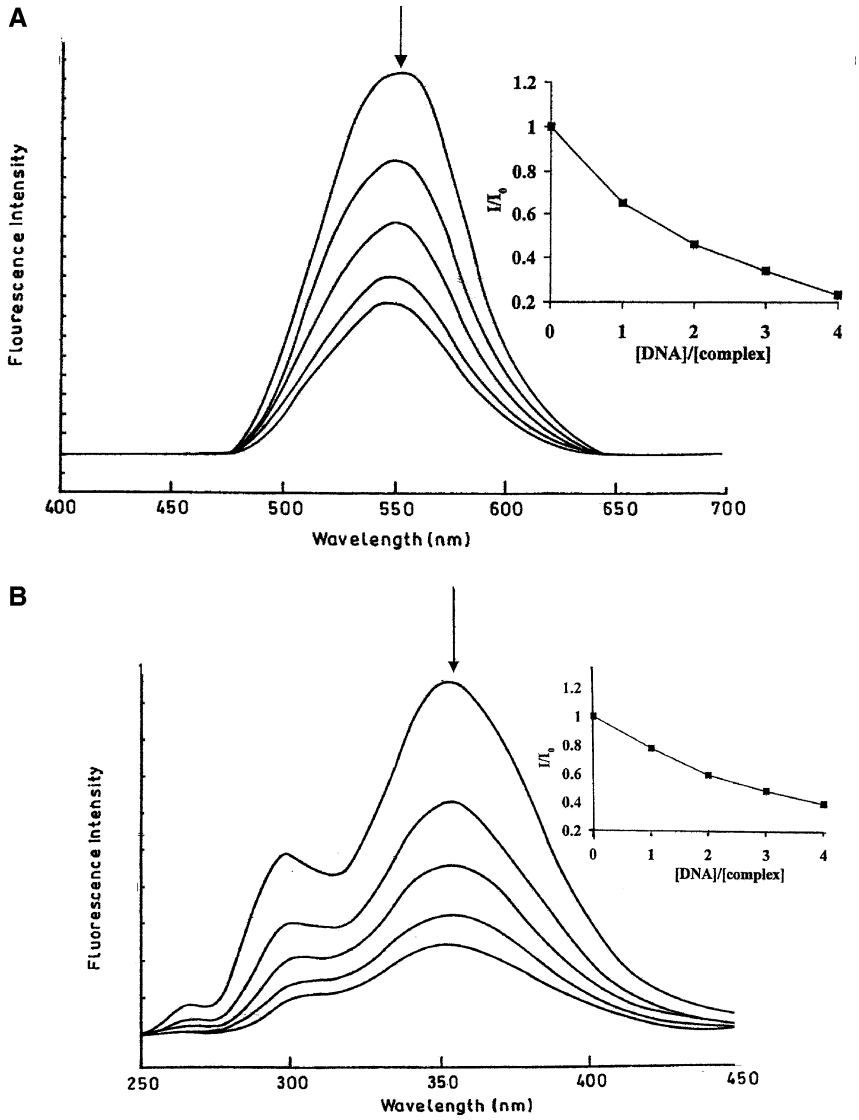


**Figure 3.** Emission spectra of (A) complex **1** and (B) complex **2** in Tris-HCl buffer DNA in the presence of DNA. [DNA] $0-13\cdot10^{-5}$ M. Arrows show the intensity changes upon increasing concentration of the complexes. Inset: Plot of relative emission intensity vs [DNA]/[complex].

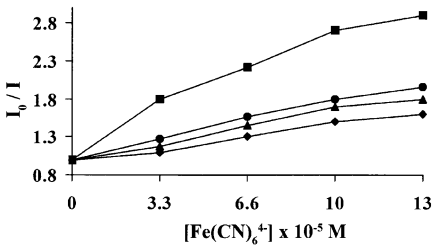


**Figure 4.** Emission quenching curve of complex **1** in absence of DNA (■) and in presence of DNA (◆) and **2** in absence of DNA (●) and in presence of DNA (▲) with increasing concentration of quencher $[Fe(CN)_6]^{4-}$. [complex] = $3.3\cdot10^{-5}$ M, [DNA] = $6.6\cdot10^{-4}$ M.

values decreased to $5\cdot10^2$ and $4\cdot10^2$ $M^{-1}$ for **1** and **2**, respectively. The greater decrease in $K_{sv}$ value of **1** in the presence of DNA as compared to **2** indicates that **1** was bound more tightly to the DNA. This could be explained by the fact that complexes free in solution or bound on the helix exterior are accessible to the quencher while those bound in the helix interior are much less accessible.[40]

**Circular Dichoric Spectral Studies.** Circular dichoric studies are useful in diagnosing changes in the morphology of DNA during complex−DNA interactions.[42] **1** and **2** were characterized by positive bands around 260 and 280 nm (Figure 5), respectively. The observed CD spectrum of CT-DNA consists of a positive band at 275 nm due to base stacking and a negative band at 245 nm due to helicity, which are characteristics of DNA in right-handed B form.[43] Simple groove binding and electrostatic interaction of the complexes with DNA show less or no perturbations on the base stacking and helicity bands while intercalator enhances the intensities of both bands.[43] The CD spectrum of CT-DNA after addition of **1** shows an increase in positive and a decrease in negative ellipticity with a red shift of 4 nm. **2** also displays a decrease and an increase in intensities, respectively, of the negative and positive bands but, interestingly, without shift in the band position. These alterations in the CD spectrum of DNA

(42) Polyanichko, A. M.; Andrushchenko, V. V.; Chikhirzhina, E. V.; Vorobev, V.; Wieser, H. *Nucleic Acids Res.* **2004**, *32*, 989−996.
(43) (a) Ivanov, V. I.; Minchenkova, L. E.; Schyolkina, A. K.; Polytayer, A. I. *Biopolymer* **1973**, *12*, 89. (b) Karidi, K.; Garoufis, A.; Tsipis, A.; Hadjiliadis, N.; Dulk, H.; Reedijik, J. *Daton Trans.* **2005**, 1176−1187.

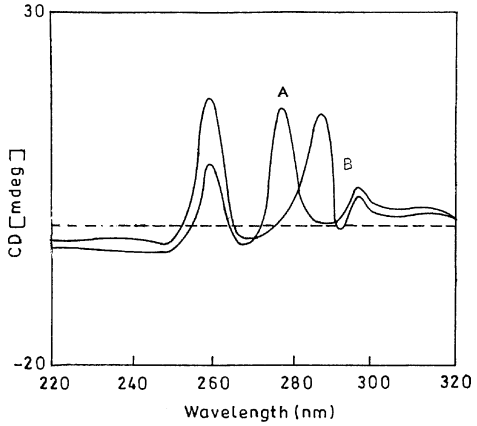


**Figure 5.** CD spectrum of (A) complex **1** and (B) complex **2**.

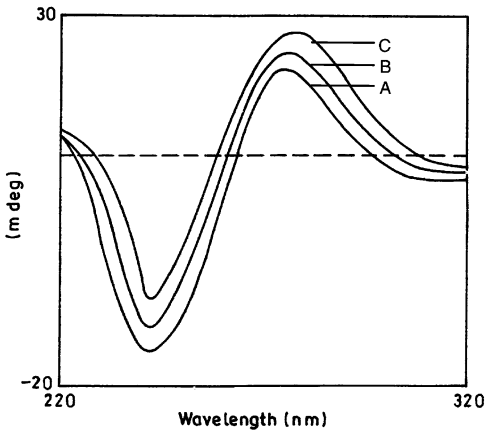


**Figure 6.** CD spectra of (A) CT-DNA alone, (B) CT-DNA in presence of complex **2**, and (C) CT-DNA in presence of complex **1** in Tris-HCl buffer at 25 °C. [complex] = $1 \cdot 10^{-4}$ M, [DNA] = $1 \cdot 10^{-4}$ M.

indicate strong conformational changes by the complexes.[44] We can see that CD spectral changes by **1** are larger than those of **2** (Figure 6). Such results suggest that the CD spectra are closely correlated with DNA binding affinity. Furthermore, the decrease in negative band is probably due to the unwinding of the DNA helix upon interaction of complexes and then transformed into other A-like conformations.

**Viscosity Studies.** Measurements of DNA viscosity are regarded as the least ambiguous and most critical test of a DNA binding model in solution[45] and affords a stronger argument for DNA binding mode.[46] The values of relative specific viscosities were plotted against $1/R$ (= [complex]/[DNA] 0.02−0.08) When **1** and **2** were treated with CT-DNA and the complex concentration increased from 0.016 to $0.064 \cdot 10^{-4}$ M. The relative specific viscosity decreases; as a consequence, it bends or kinks the DNA helix, which is attributed to the strong covalent binding of complexes with DNA bases.[47]

**Cyclic Voltammetry (CV).** The electrochemical profiles of **1** and **2** were studied in $H_2O$/DMSO (95:5) by cyclic voltammetry in the range from 2.0 to −0.8 V. Both the complexes displayed a well-defined cathodic wave, but the corresponding anodic waves were drawn out revealing that the very unstable $Cu^I$ species are not discernible with the time scale of the CV experiments.[48] The cyclic voltammogram of **1** exhibited quasi-reversible one-electron redox process involving the $Cu^{II}/Cu^I$ couple with cathodic peak at $E_{pc}$= −0.45 V and oxidation peak $E_{pa}$ = −0.31V (Figure 7). For this couple, the difference between cathodic and anodic peak potential $\Delta E_p$ and ratio of anodic and cathodic peak currents $I_{pa}/I_{pc}$ are −0.140 V and ∼1, respectively. The formal electrode potential $E_{1/2}$ taken as an average of $E_{pc}$ and $E_{pa}$ was −0.38 V in the absence of DNA. The CV of **2** featured reduction of the $Cu^{II}/Cu^I$ form at a cathodic peak potential $E_{pc}$ of −0.42 V. Reoxidation of the complex occurred at −0.32 V. The separation of the anodic and cathodic peak potential $\Delta E_p$ = −0.10 V and $I_{pa}/I_{pc}$ ratio = 0.43 indicated a quasi-reversible redox process.

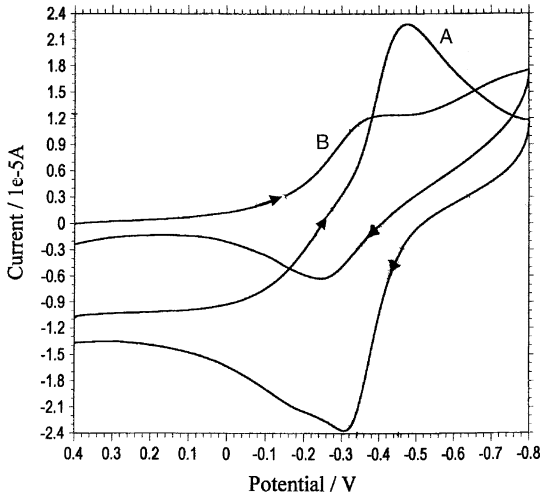


**Figure 7.** Cyclic voltammogram (5:95 DMSO/$H_2O$, 25 °C) of (A) unbound complex **1** and (B) complex **1** in presence of CT-DNA. [complex **1**] $1 \cdot 10^{-3}$ M, [DNA] $6 \cdot 10^{-3}$ M.

Addition of CT-DNA to **1** and **2** results in significant reduction in cathodic and anodic peak current due to slow diffusion of an equilibrium mixture of the free and DNA-bound complexes to the electrode surface.[49] The observed shifts in $E_{1/2}$ values to less negative potentials suggest that $Cu^{II}$ and $Cu^I$ forms of **1** and **2** bind to DNA. However, the larger shift in $\Delta E_p$, $E_{1/2}$, and $I_{pa}/I_{pc}$ values observed for **1** than that of **2** upon addition of CT-DNA may suggest that the binding affinity of the former to DNA is stronger than that of the latter.[50]

**In Vitro Antitumor Studies.** The molecular design of novel chiral complex **1** is very unique as it provides distinct

(44) Tamilselvi, P.; Palaniandavar, M. *Inorg. Chim. Acta* **2002**, *337*, 420−428.
(45) Satyanaryana, S.; Dabrowaik, J. C.; Chairs, J. B. *Biochemistry* **1993**, *32*, 2573−2584. (b) Plish, D. S.; Waring, M. J.; Sun, J. S.; Rougee, M.; Nguyen, C. H.; Bisagni, E.; Garestier, T.; Helene, C. *J. Mol. Biol.* **1993**, *232*, 926−946.
(46) Norden, B.; Tejerneld, T. *Biopolymer* **1982**, *21*, 1713−1734.
(47) (a) Maheswari, P. U.; Palaniandavar, M. *J. Inorg. Biochem.* **2004**, *98*, 219−230. (b) Tabassum, S.; Mathur, S. *J. Carbohydr. Chem.* **2005**, *24*, 865−887. (c) Liu, J.; Lu, T. B.; Li, H.; Zhang, Q. L.; Ji, L. N. *Transition Met. Chem.* **2002**, *27*, 686−690.
(48) (a) Raja, A.; Rajendiran, V.; Maheswari, P. U.; Balamurugan, R.; Kilner, C. A.; Halcrow, M. A.; Palaniandavar, M. *J. Inorg. Biochem.* **2005**, *99*, 1717−1732. (b) Baguley, B. C.; LeBert, M. *Biochemistry* **1984**, *23*, 937−943.
(49) Liu, J.; Zhang, T.; Lu, T.; Qu, L.; Zhou, H.; Zhang, Q.; Ji, L. *J. Inorg. Biochem.* **2002**, *91*, 269−276.
(50) Yang, Z. S.; Wang, Y. L.; Liu, Y. C.; Zhao, G. C. *Anal. Sci.* **2005**, *21*, 1355−1358.

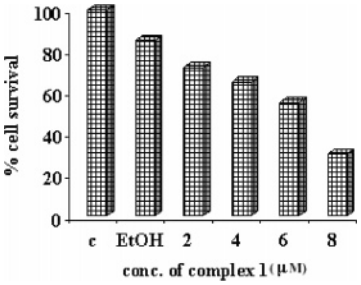


**Figure 8.** Effect of complex **1** on SY5Y proliferation after 24 h of treatment.

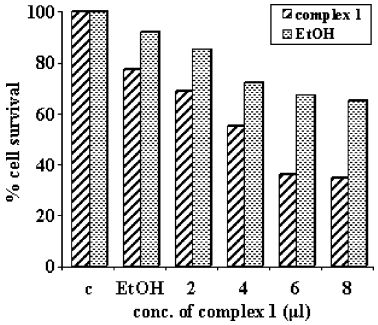


**Figure 9.** Dose-dependent cytotoxic effect of complex **1** toward SY5Y cells. After 24 h, cell viability was evaluated by MTT assay. Data expressed as a percentage of the control MTT reduction. Since complex **1** is EtOH-soluble, cells treated with EtOH without complex **1** were used as controls.

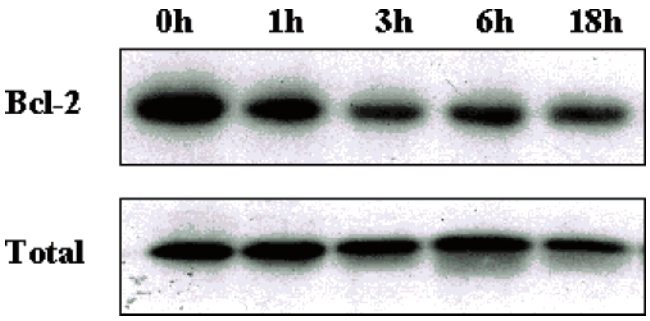


**Figure 10.** Protein levels of Bcl-2 determined through Western blotting using total cell lysates of SY5Y cells after treatment with 2 $\mu$L of complex **1**. Controls were used to ensure equal protein loading. Protein after lane 1, 0 h; lane 2, 1 h; lane 3, 3 h; lane 4, 6 h; lane 5, 18 h of treatment with complex **1**.

recognition properties for biopolymer structure. **1** contains two metal centers, a $Cu^{II}$ and $Sn^{IV}$ metal ion, which act in accord with each other to distort the DNA structure. Previous reports reveal that the $Sn^{IV}$ cation interacts with the phosphate backbone of the DNA double helix and influences the growth of tumor cells. Thus, the mechanism of antitumor action of $Sn^{IV}$ complexes substantially differs from classical anticancer drugs (cisplatin) and modulatory activity of transition metal ions in presence of tin is a unique way to address resistance of the anticancer drugs. Complex **1** was selected for antitumor activity in vitro because it exhibited higher activity than that of **2** in preliminary DNA binding studies. To investigate the antitumor activity of **1**, cell counting, MTT assay, Western blot analysis, and caspase activity were performed.

**Effects on Cell Proliferation.** The growth inhibitory effect of **1** was examined in SY5Y and PC-12 cells using untreated cells as negative controls. In both cases drug treatment in the concentration range between 2 and 8 $\mu$M resulted in a dose-dependent inhibition of cell survival. The results of this experiment on SY5Y are shown in Figure 8. As can be seen, **1** showed good antitumor activity toward both cell lines. In SY5Y and PC-12 cells a progressive decrease of cell survival was observed after 24 h for **1**, when the drug concentration increased. Note that the relative number of live PC-12 cells was lower than those of the SY5Y cell line.[51] Such differences in cell viability may be perhaps due to the different origin of the PC-12 cells, a pheochromocytoma cancer cell line, which are undifferentiated cells in comparison to SY5Y cells, a human neuroblastoma cancer cell line.

**Cytotoxicity of Complex 1.** The in vitro cytotoxicity effect of **1** against SY5Y tumor cells was analyzed by MTT assay, which serves as an index of cell viability by measuring the reduction of tetrazolium salt to a blue formazan product by mitochondrial enzyme activity of succinate dehydrogenase in living cells.[52] Complex **1** in the range of 2.0−8.0 $\mu$M caused dose-dependent cytotoxicity with approximately 50% of the cells having lost viability after **1** treatment at a concentration of 4 $\mu$M as shown in Figure 9. These results are in accordance with those of the counting experiments.[51]

**Complex 1-Induced Apoptosis in SY5Y Cells by Intrinsic Mitochondrial Pathway.** The Bcl-2 family of proteins regulates apoptosis by controlling mitochondrial permeability and the release of cytochrome *c* (cyto c). The anti-apoptosis proteins Bcl-2 and Bcl-xL reside in the outer mitochondrial wall and inhibit cyto c release. The pro-apoptotic Bcl-2 proteins Bad, Bax, and Bak reside in the cytosol but translocate to mitochondria following death, signaling where they promote the release of cyto c[53]

**Reduced Bcl-2 Protein Level in Response to 1 Treatment in SY5Y Cells.** To investigate the role of anti-apoptotic members of the Bcl-2 family in the induction of apoptosis in SY5Y cells, we determined its expression in untreated and complex **1**-treated cells by Western blot analysis of total cell extracts. As shown in Figure 10, **1** provoked a lower level of expression of Bcl-2 in SY5Y cells as measured at a fixed dose of **1** (2 $\mu$L) with different time points. Decline in Bcl-2 level was time-dependent and was maximum after 24 h of treatment with **1**. These results support that **1** induced apoptosis associated with a reduced Bcl-2 protein level.[54]

**Bak Expression in SY5Y Cells after Incubation with 1.** The most intuitive link between p53-mediated transactivation and apoptosis comes from the ability of p53 to control transcription of proapoptotic members of Bcl-2 family. To determine whether p53 is involved in complex **1**-induced apoptosis, we examined the expression of its direct downstream factor Bak. SY5Y cells were treated with 2.0 $\mu$g/mL of **1**, harvested at different time points. Mitochondrial proteins were extracted, which were then subjected to

(51) Katsaros, N.; Katsarou, M.; Sovilj, S. P.; Samardzija, K. B.; Mitic, D. M. *Bioinorg. Chem. Appl.* **2004**, *2*, 193−207.
(52) Buttke, T. M.; Sandstrom, P. A. *Immunol. Today* **1994**, *15*, 7−10.
(53) Tsujimoto, Y.; Shimizu, S. *FEBS. Lett.* **2000**, *466*, 6−10.
(54) Tsai, H. F.; Tsai, H. J.; Hsieh, M. *Biochem. Biophy. Res. Commun.* **2004**, *324*, 1274−1282.

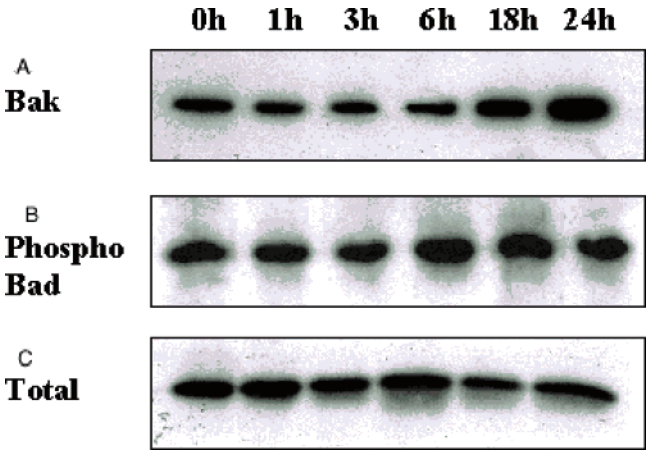


**Figure 11.** Immunoblot analysis of (A) Bak, (B) phospho-bad, and (C) total bad in mitochondrial lysates of SY5Y cells at indicated time treated with 2 $\mu$L of complex **1**.

Western blot analysis with anti-Bak antibody as depicted in Figure 11A. Expression level of the Bak in SY5Y cells were shown to increase as the incubation time proceeded after the treatment of **1**.[55] Since it is well-known that proapoptotic proteins promotes cell death induced by a variety of stimuli, so up-regulation of Bak is evidence of **1**-induced apoptosis.

**Bad Regulation in Apoptotic SY5Y Cells.** The proapoptotic Bcl-2 family protein Bad resides in the cytosol but translocates to mitochondria following death, signaling where they promote the release of cyto c. Bad translocates to mitochondria and forms proapoptotic complex with Bcl-xL. This translocation is inhibited by survival factors that induce phosphorylation of Bad, leading to its cytosolic sequestration.[56] Phosphorylated Bad was seen only in control (Figure 11B). No Bad was seen even at earliest time point of 1 h of **1** treatment, indicating inhibition of phosphorylation of Bad. No difference was seen in the total levels of Bad in mitochondria (Figure 11C).

**Role of p53 in 1-Induced Apoptosis.** The p53 tumor suppressor gene is the most frequently mutated gene in human cancer. Activation of p53 can lead to either cell cycle arrest and DNA repair or apoptosis. p53 is phosphorylated at multiple sites in vivo and by several different protein kinases in vitro. DNA damage induces phosphorylation of p53 at Ser15 and Ser20 and leads to reduce interaction of p53 with its negative regulator, oncoprotein murine double minute 2 (MDM2). MDM2 inhibits the accumulation of p53 by targeting it for ubiquitination and proteazomal degradation. p53 can apparently be phosphorylated by ATM, ATR, and DNA-PK at Ser15. This phosphorylation impairs the ability of MDM2 to bind p53, promoting both the accumulation and functional activation of p53 in response to DNA damage.

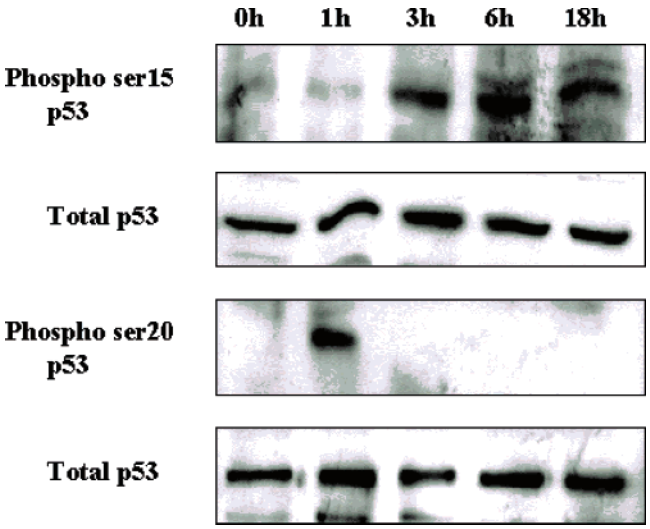


**Figure 12.** Expression of p-53 proteins. Western blot analysis of nuclear cell extracts of SY5Y cells at different time points after treatment with 2 $\mu$L of complex **1**.

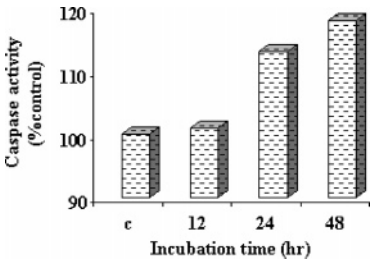


**Figure 13.** Caspase activity induced by complex **1** (2 $\mu$L) in SY5Y cells at 0−48 h was expressed as a percentage of the 0-h time value.

This section examines whether p53 protein is involved in **1**-induced apoptosis. The p53 activity was studied by extracting nuclear protein from **1**-treated cells and monitoring the p53 protein by immunoblot analysis. The p53 protein was detectable in the nuclear extract of the untreated cells (Figure 12, lane 1). After an exposure to **1**, the p53 (phospho-Ser15 and phospho-Ser20) protein level was elevated in a time-dependent manner. A **1**-induced increase in phospho-Ser15 and phospho-Ser20 was not noticeable at 1, 3, and 6 h (Figure 12, lanes 2−4), and this increase reached its peak at 18 h (Figure 12, lane 5) during the period of **1** treatment. However, there was no change in the total p-53 on treatment with **1**. Collectively, these results demonstrate that p-53 was activated by **1** because nuclear p-53 level was increased.

**1-Induced Cell Death Requires Caspase-3 Activation.** Caspases have been reported to play vital roles in executing apoptosis.[57] To identify the role of caspase involved in the signaling of apoptosis induced by **1**, we examined protein level of active caspase-3 (Figure 13). Incubation of 12 h with **1** (2.0 $\mu$L/mL) increased the protein level of caspase-3 to 101% of the control. However, incubating SY5Y cells with **1** for 24 h resulted in an increase of caspase-3 to 113% of the control while 48 h incubation with **1** increased the protein level 118% to that of control cells.

(55) (a) Pearson, A. S.; Francis, R.; Spitz, S.; Swisher, G.; Masafumi, K.; Mona, G. S.; Meyn, R. E.; McDonnell, T. J.; Cristiano, R. J.; Roth, J. A. *Clin. Cancer. Res.* **2000**, *6*, 887−890. (b) Yuan, J.; Lovejoy, D. B.; Richardson, D. R. *Blood* **2004**, *104*, 1450−1458.

(56) (a) Tao, W.; Kurschner, C.; Morgan, J. I. *J. Biol. Chem.* **1998**, *273*, 23704−23708. (b) Zha, J.; Harada, H.; Yang, E.; Jockel, J.; Korsmeyer, S. J. *Cell* **1996**, *87*, 619−628.

(57) (a) Cohen, G. M. *Biochem. J.* **1997**, *326*, 1−16. (b) Earnshaw, W. C.; Martins, L. M.; Kaufmann, S. H. *Annu. Rev. Biochem.* **1999**, *68*, 383−424.

## Conclusions

The synthesis and structural characterization of $Sn^{IV}/Zr^{IV}$ modulated $Cu^{II}/Zn^{II}$ trinuclear **1**−**4** were carried out with an aim to develop robust cancer chemotherapeutic agents. DNA binding experiments with **1** and **2** were employed (viz. electronic and emission spectral, viscometric and electrochemical studies). Preliminary DNA binding experiments of **1** and **2** reveal that **1** binds to DNA more strongly than **2** due to the presence of the $Sn^{IV}$ metal ion, which has more Lewis acid character than the zirconium metal ion. In vitro antitumor activity of **1** further justifies its potent antitumor effect, which is capable of inhibiting the growth of SY5Y by 60% at 8 $\mu$M and of PC-12 by 70% at 2 $\mu$M. In the case of the SY5Y neuroblastoma cell line, **1** exhibits significant antiproliferative activity indicative of apoptosis. The immunoblot analysis demonstrated that mitochondrion play a key role in governing the induction of apoptosis by **1**. This is further diagnosed by the activation of caspase-3. Indeed, **1** is one of the most effective antitumor agents developed in terms of its selective antitumor activity, and it warrants further vigorous investigations.

**Acknowledgment.** C.S.I.R. (01 (1982)/05-EMR-II) and UGC (F 12-21/2003(SR), New Delhi, India, are acknowledged for funding. Thanks to RSIC, CDRI, Lucknow, for providing CHN analysis data, NMR, and polarimetery and to IIT Bombay for EPR measurements. The authors gratefully acknowledge Prof. Sartaj Tabassum and Dr. Rizwan H Khan, A.M.U, Aligarh, for his valuable suggestions in designing antitumour experiments and for providing the CD facility, respectively. Our thanks to Prof. Claudio Pettinari, Department of Chemistry, University di Camerino, Italy, for $^{119}Sn$ NMR.

**Supporting Information Available:** Figures showing the EPR spectra of complexes **1** and **2** in solution and solid state, cyclic voltammogram of complex **2** in absence and in presence of DNA, effect of complexes **1** and **2** on the viscosity of DNA, and effect of complex **1** on PC-12 proliferation after 24 h of treatment. This material is available free of charge via the Internet at http://pubs.acs.org.

IC061753A